

# A Continuum Model of Continental Deformation Above Subduction Zones: Application to the Andes and the Aegean

SHIMON WDOWINSKI AND RICHARD J. O'CONNELL

*Department of Earth and Planetary Sciences, Harvard University, Cambridge, Massachusetts*

PHILIP ENGLAND

*Department of Earth Sciences, Oxford University, Oxford, England*

Large-scale continental tectonics of back arc (extensional) and Andean-type (compressional) environments are investigated by using the thin viscous sheet model to calculate the deformation within continental lithosphere that is subjected to horizontal forces on its plate boundaries and to basal drag from the asthenospheric flow beneath. The shear tractions acting on the base of a deformable lithosphere are derived from a corner flow model that assumes a rigid subducting plate and a deformable overlying plate. Because the calculated shear tractions and the deformation within the overlying plate are interdependent, the corner flow and the thin viscous sheet models are solved simultaneously. We use a perturbation method to obtain analytical solutions for the velocity and strain rate fields within the overlying continental lithosphere. The solutions depend on the angle of subduction, the dimensionless thickness of the lithosphere, and the ratio of asthenospheric to lithospheric viscosities, which governs the viscous coupling between the asthenosphere and the lithosphere. Calculations are compared with observations from the Andes and the Aegean; our results explain some of the features of the deformation in these regions that have heretofore not been explained by other models. Our model predicts that in a compressional environment a broad region of uplifted topography will tend to develop above a more steeply dipping slab ( $30^\circ$ ), rather than above a shallower slab ( $10^\circ$ – $15^\circ$ ); this is in accord with observations in the various segments of the central Andes. For an extensional environment, the model predicts that a zone of compression can develop near the trench and that extensional strain rate can increase with distance from the trench, as is observed in the Aegean. We also estimate the effective viscosities of  $\sim 10^{20}$  Pa s for the asthenosphere,  $\sim 2 \times 10^{21}$  Pa s for the Aegean lithosphere, and  $\sim 10^{22}$  Pa s for the Andean lithosphere.

## INTRODUCTION

Subducting plate boundaries are the most tectonically active regions on Earth. Though seismicity indicates that processes within sinking slabs are similar everywhere, the deformation of the overlying plate can vary greatly. The large-scale deformation can be either compressional, as in the Andes, or extensional, as in the Aegean or other back arc basins. Furthermore, the overriding plate in a back arc environment may exhibit large-scale extensional and compressional stress fields at short distances from one another. A narrow belt along the trench is subjected to compression, while further from the trench the plate extends either by interplate deformation or by the initiation of a spreading center.

It has been long noticed that subduction plate boundaries can be classified into two types according to their tectonic stress field: extensional (back arc) and compressional [e.g., *Wilson and Burke, 1972; Uyeda and Kanamori, 1979*]. Some of the explanations of the first-order deformation are the convergence rate between the overriding and the subducting plates [*Hyndman, 1972*], age of the subducting plate [*Molnar and Atwater, 1978*], and the geometry of the subduction zones [e.g., *Uyeda and Kanamori, 1979*]. Investigations of global mantle flow suggest that global plate motion strongly

influences the type of deformation above subduction zones [e.g., *Hager et al., 1983*].

A common explanation for mountain building processes above subduction zones is strong mechanical coupling between upper and lower plates where the subduction is very shallow (Chilean-type subduction) [e.g., *Uyeda and Kanamori, 1979*]. However, the widest Andean plateau is located above a relatively steeply dipping slab [*Stauder, 1975; Barazangi and Isacks, 1976*], where the contact between the subducting and overriding plates is limited to a narrow zone near the trench. *Isacks [1988]* explains the formation of the Andes as a result of horizontal shortening preceded by a thermal weakening event. He suggests that the horizontal extent of the various segments of the Andes are independent of the present-day geometry and represent the subduction geometry during the weakening event.

The Aegean deformation is characterized by compression near the trench, minor extension in the southern Aegean, and intensive extension in the northern Aegean [*McKenzie, 1978; Jackson and McKenzie, 1988*]. So far there is no single model that explains the observed Aegean deformation. *McKenzie [1978]* used a corner flow model, where the subducting and overlying plates are rigid, to explain the compression near the trench; but because the overriding plate was assumed to be rigid he was unable to explain the distribution of the extension. *Sonder and England [1989]* used a thin viscous sheet model with temperature dependent rheology overlying an inviscid asthenosphere to explain the spatial distribution of the extension, but this model does not produce compression near the trench.

Copyright 1989 by the American Geophysical Union.

Paper number 89JB00913.  
0148-0227/89/89JB-00913\$05.00

We present here a simple model that can encompass the first- and second-order large-scale deformation above subduction zones. Continental lithosphere overlying a subduction zone can be treated as a continuum deforming over a geological time period. This assumption enables us to solve for the deformation as a boundary value problem. The boundary conditions, which determine the first-order deformation, are taken from the well-constrained global plate velocity models [e.g., *Minster and Jordan, 1978; Chase, 1978*]. Since plate tectonics is a kinematic theory, we cannot explain the cause of the first-order deformation, but it enables us to describe the deformation quantitatively. Shear traction acting on the base of the lithosphere is an additional boundary condition that is calculated from a corner flow model for the asthenosphere below the lithosphere and which causes the second-order deformation of the lithosphere. This boundary value formulation gives us a quantitative description of the deformation above subduction zones that includes the most important mechanisms: global plate motion and local interaction between the lithosphere and the asthenosphere.

### THE MODEL

Our model (Figure 1) is a combination of two previous models: a thin viscous sheet model of the lithosphere [*England and McKenzie, 1982*] and a model that treats the flow in the asthenosphere near a subducting plate as a corner flow [*McKenzie, 1969, 1978*]. These models are modified and combined to provide a physical representation of a subduction zone. The model assumes that the apex of the asthenospheric wedge and the edge of lithosphere are at the same horizontal position, which we identify with the trench. This explicitly ignores the region that lies between the trench and the tip of the asthenospheric wedge (stippled in Figure 1).

The shape of subduction zones makes it reasonable to neglect variations in the along-strike direction. We use the thin viscous sheet model because it appears to describe continental lithospheric deformation quantitatively [*England and McKenzie, 1982; Houseman and England, 1986; Sonder et al., 1986*]. The advantage of the thin sheet approximation is that velocities and stresses are vertically averaged, which

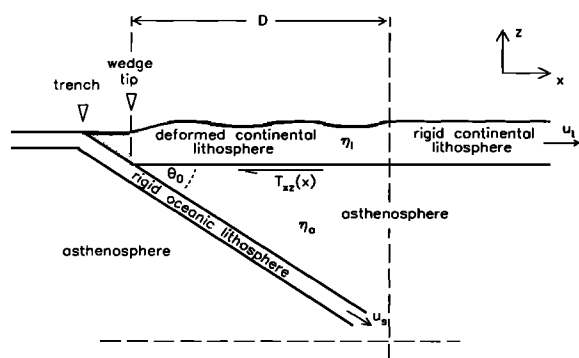


Fig. 1. Schematic diagram of the model showing the geometry and the parameters that influence the deformation of a continental lithosphere above subduction zone.  $D$  is the width of the zone of deformation;  $\eta_l$ , the lithospheric viscosity;  $\eta_o$ , the asthenospheric viscosity;  $T_{xz}(x)$ , the basal drag;  $\theta_0$ , the angle of subduction;  $u_s$ , the subduction velocity; and  $u_t$ , the trench velocity. The dashed lines represent the lateral and vertical extent of the model.

eliminates the vertical dimension from the mathematical formulation. Thus, the mathematical formulation of the two-dimensional flow reduces the boundary value problem to one dimension only. Another modification of the model is consideration of shear traction on the base of the lithosphere, similar to the plane stress model of *Bird and Baumgardner [1984]*. However, when shear tractions are present, the thin sheet solutions, which are vertically averaged, are less accurate; the order of accuracy, which is evaluated in the appendix, depends on the wavelength of the dominant shear traction and the thickness of the lithosphere.

Corner flow models have been used to describe asthenosphere flow in subduction zones. Some models treat the asthenosphere as a Newtonian fluid [e.g., *McKenzie, 1969, 1978; Sleep and Toksöz, 1971; Stevenson and Turner, 1977*], while others calculate corner flow for a nonlinear rheology as well [*Tovish et al., 1978*]. All of these models use the classical corner flow models of *Moffat [1964]* and *Batchelor [1967]*, where the flow is bounded by two rigid plates. Observations from subduction zones show that both bounding plates are deforming. Seismicity indicates limited deformation within the subducting oceanic lithosphere, but the overriding continental lithosphere is often extensively deformed. Therefore, we assume that the corner flow is bounded by an inclined rigid plate and deformable overlying plate. Mathematically, the corner flow model is applicable to an infinite wedge. Since the physical problem has finite dimensions, we limit our region of interest to the wedge that lies beneath the deformed part of the overlying plate and above the entire length of the subducting slab (Figure 1).

For calculating the deformation of the lithosphere, we need the shear traction at the base of the lithosphere that results from flow in the asthenospheric wedge. The basal shear traction determines the deformation of the overlying plate; in turn, the shear traction depends on the deformation. Thus, the corner flow and the thin viscous sheet models are solved simultaneously for velocity and stress fields within the lithosphere and the asthenosphere below.

### Model of Two-Dimensional Thin Viscous Sheet With Basal Shear Traction

We follow most of the thin viscous sheet assumptions described in detail by *England and McKenzie [1982]* and *England et al. [1985]*. First, we assume that the continental lithosphere behaves as an incompressible viscous fluid deforming by steady state creep over geological time periods. The force balance equation for two-dimensional flow with zero Reynolds number is

$$\sigma_{ij,j} = \rho g a_i \quad (1)$$

where  $\sigma_{ij}$  is the  $(i, j)$  component of the stress tensor,  $\rho$  is the density,  $g$  is the acceleration due to gravity, and  $a = (0, 1)$ . The deviatoric stress tensor is

$$\tau_{ij} = \sigma_{ij} + \delta_{ij} p \quad (2)$$

where  $p$  is the pressure ( $p = -\frac{1}{3}\sigma_{kk}$ ).

The thin sheet approximation assumes that the horizontal gradients of the stresses are negligible with respect to the vertical gradients. We use this approximation and integrate the vertical component of (1) with respect to depth from the top of the thin sheet ( $z = z_t$ ) downward; thus

$$\sigma_{zz} = - \int_z^{z_t} \rho g dz' \quad (3)$$

Then, using (2) we integrate the horizontal component of (1) with respect to depth from the the bottom ( $z = z_b$ ) to top of the layer ( $z = z_t$ ). In addition, we assume that the upper surface is traction free and that the bottom surface is at a constant depth and is subjected to shear traction; thus

$$\frac{\partial}{\partial x} \int_{z_b}^{z_t} (\tau_{xx} - p) dz + T_{xz}^b = 0 \quad (4)$$

where  $T_{xz}^b$  is the shear traction acting on the base of the layer. We use the vertical component of (2) and the incompressibility condition ( $\tau_{xx} = -\tau_{zz}$ ) to eliminate  $p$  in (4); thus

$$2L \frac{d\bar{\tau}_{xx}}{dx} = -L \frac{d\bar{\sigma}_{zz}}{dx} - T_{xz}^b \quad (5)$$

where  $L$  is the thickness of the layer ( $L = z_t - z_b$ ),  $\bar{\tau}$  is the vertically averaged deviatoric stress, and  $\bar{\sigma}_{zz}$  is the vertically averaged vertical stress that can be evaluated from the density structure of the lithosphere. We adopt a Newtonian rheology for the thin sheet, which therefore has the constitutive relation

$$\bar{\tau}_{ij} = 2\eta \dot{\epsilon}_{ij} \quad (6)$$

where  $\eta$  is the viscosity and  $\dot{\epsilon}_{ij}$  is a component of the vertically averaged strain rate tensor which is defined by

$$\dot{\epsilon}_{ij} = \frac{1}{2} (u_{i,j} + u_{j,i}) \quad (7)$$

where  $u_i$  is a component of the vertically averaged velocity vector.

We substitute (6) and (7) into (5) and assume local isostatic compensation on the base of the lithosphere. We also assume that the lithosphere consists of a crust of thickness  $S$  and density  $\rho_c$  overlying a mantle of density  $\rho_m$ . In nondimensional variables, we get

$$4L\eta \frac{d^2 u}{dx^2} = Ar \frac{d(S^2)}{dx} - T_{xz}^d \quad (8)$$

where  $x$ ,  $u$ , and  $\eta$  are now the nondimensional length, velocity, and viscosity, respectively. The characteristic length scale  $D$  is the width of the zone of deformation (Figure 1); velocity scale  $u_s$  is the subduction velocity; and the viscosity is scaled to the lithospheric viscosity  $\eta$ . This defines the time scale as  $D/u_s$ .  $L$  and  $S$  are the dimensionless thickness of the lithosphere and the crust, respectively.  $T_{xz}^d$  is the dimensionless shear traction acting on the base of the layer, and  $Ar$  is

$$Ar = \frac{g\rho_c D^2}{2\eta u_s} \left( 1 - \frac{\rho_c}{\rho_m} \right) \quad (9)$$

It is similar to the Argand number of *England and McKenzie* [1982], which measures the contribution of the buoyancy forces arising from lateral variations of crustal thickness. The difference between the two  $Ar$  definitions arises from a different choice of the characteristic length scale (we use the width of the zone of deformation ( $D$ ) and *England and McKenzie* [1982] use the lithospheric thickness ( $L$ )). In order to simplify the equation and to limit the number of degrees of freedom in our calculations, we assume no variations in crustal thickness and omit the buoyancy force term.

Thus, the governing equation reduces to

$$4L\eta \frac{d^2 u}{dx^2} = -T_{xz}^d \quad (10)$$

By using the thin sheet approximation, the boundary value problem is reduced to a second-order ordinary differential equation that requires two boundary conditions. Since the plate tectonic framework provides constraints on the velocities rather than stresses of plates, kinematic boundary conditions are most convenient. There are two velocities that must be considered: the convergent velocity between two adjacent (rigid) plates on both sides of the trench and the velocity of trench migration relative to the rigid part of the overlying plate [*Karig*, 1971; *Forsyth and Uyeda*, 1975].

We choose the width of the zone of deformation  $D$  (Figure 1) as the characteristic length scale and use dimensionless coordinates ( $x$ ), where the wedge tip is the origin ( $x = 0$ ). The region in which the continental lithosphere is deformed is our region of interest ( $0 < x < 1$ ). Farther away ( $x > 1$ ), the continental lithosphere is not deforming and moves as a rigid plate with respect to the wedge tip. The velocity of the rigid plate relative to the wedge tip ( $u_t$ ) is the sum of the relative plate motion and trench migration velocities. We use the subduction velocity ( $u_s$ ) as the characteristic velocity. Hence, the dimensionless boundary conditions that result from our frame of reference are (1) zero velocity at the wedge tip  $u(0) = 0$  (the edge of the continental lithosphere is always at the wedge tip (trench), so no holes open up) and (2) fixed velocity of the overlying plate far from the trench  $u(1) = u_0$  ( $u_0 = u_t/u_s$ ) where  $u_0$  is the relative plate motion plus trench migration.

#### Corner Flow With a Deformable Bounding Plate

We follow the formulation of *Fenner* [1975]. For incompressible two-dimensional flow, a stream function in polar coordinates gives

$$\begin{aligned} u_r &= \frac{1}{r} \psi_{,\theta} \\ u_\theta &= -\psi_{,r} \end{aligned} \quad (11)$$

where  $(u_r, u_\theta)$  are the velocity components in polar coordinates  $(r, \theta)$ . There is a singularity at the origin which will be considered later. For steady, homogeneous, slow Newtonian flows, the equation of motion reduces to the biharmonic equation

$$\nabla^4 \psi = 0 \quad (12)$$

We seek a separable solution [*Moffat*, 1964; *Fenner*, 1975] of the form

$$\psi = r^n T_n(\theta) \quad (13)$$

where  $n$  may be any real power of  $r$  [ $0 \leq r \leq 1$ ] but for our purposes it is sufficient to use integer values only, and  $T_n(\theta)$  is given in terms of four arbitrary constants  $A$ ,  $B$ ,  $C$  and  $D$ .

For  $n = 0$  or  $n = 2$ ,

$$T_0(\theta) = T_2(\theta) = A \cos 2\theta + B \sin 2\theta + C\theta + D \quad (14)$$

for  $n = 1$ ,

$$T_1(\theta) = A \cos \theta + B \sin \theta + C\theta \cos \theta + D\theta \sin \theta \quad (15)$$

and for any other value of  $n$ ,

$$T_n(\theta) = A \cos n\theta + B \sin n\theta + C \cos(n-2)\theta + D \sin(n-2)\theta \quad (16)$$

In general, an infinite series of terms of the form of (13) is required to satisfy all the boundary conditions. Thus,

$$\psi = \sum_{n=0}^{\infty} K_n r^n T_n(\theta) \quad (17)$$

where the  $K_n$  are constants chosen to satisfy the boundary conditions.

As discussed previously, the coordinate system is fixed with respect to the wedge tip. The subducting oceanic plate is assumed to be rigid, and it subducts at a constant velocity ( $u_r = 1$ ;  $u_\theta = 0$ ) which is scaled to the subduction velocity  $u_s$ . The overlying plate is fixed at the wedge tip  $u(0) = 0$  but may deform elsewhere. In the case of Newtonian flow, we can separate the boundary value problem into two simpler problems as described in Figure 2. We solve the two problems separately and add the results to get the solution for the corner flow with a rigid subducting plate and an overlying deformable plate.

*Problem 1 (Figure 2b).* This is the classical corner flow problem for two rigid plates. The overlying plate is fixed and the inclined plate moves downward at constant velocity  $u_s$ . The solution for this problem is given by Moffat [1964], Batchelor [1967], and McKenzie [1969]. We represent the solution in the form of McKenzie [1969]:

$$\psi(r, \theta) = r \frac{(\theta_0 - \theta) \sin \theta_0 \sin \theta - \theta_0 \theta \sin(\theta_0 - \theta)}{\theta_0^2 - \sin^2 \theta_0} \quad (18)$$

where  $\theta_0$  is the angle of subduction ( $0 < \theta_0 \leq \pi/2$ ).

*Problem 2 (Figure 2c).* This is the boundary value problem for corner flow with a fixed inclined plate and a deformable overlying plate. The solution must satisfy the following boundary conditions:

At  $\theta = 0$

$$\psi_{,r} = 0 \quad (19a)$$

$$\frac{1}{r} \psi_{,\theta} = f(r) \quad (19b)$$

At  $\theta = \theta_0$

$$\psi_{,r} = 0 \quad (20a)$$

$$\frac{1}{r} \psi_{,\theta} = 0 \quad (20b)$$

where  $f(r)$  is the velocity within the overlying plate. We represent  $f(r)$  as a power series:

$$f(r) = \sum_{n=1}^{\infty} a_n r^n \quad (21)$$

where  $a_n$  is the dimensionless velocity coefficient that is scaled to the subduction velocity  $u_s$ .

Substituting (17) and (21) into the boundary condition (19b), we find that the stream function has the following form:

$$\psi(r, \theta) = \sum_{n=2}^{\infty} \frac{a_{n-1}}{T'_n(0)} r^n T_n(\theta) \quad (22)$$

where  $a_{n-1}$  are given by the velocity boundary conditions.  $T'_n(0)$ , the first derivative of  $T(\theta)$  evaluated at  $\theta = 0$ , can be found by using the other boundary conditions (equations (19a), (20a), and (20b)).

*Calculation of the basal shear traction.* Combining the solutions of (18) and (22), we get a stream function expression that satisfies all the boundary conditions:

$$\psi(r, \theta) = \sum_{n=2}^{\infty} \frac{a_{n-1}}{T'_n(0)} r^n T_n(\theta) + r \frac{(\theta_0 - \theta) \sin \theta_0 \sin \theta - \theta_0 \theta \sin(\theta_0 - \theta)}{\theta_0^2 - \sin^2 \theta_0} \quad (23)$$

From this, the shear traction on the base of the lithosphere can be derived easily. For Newtonian fluids the shear stress is

$$\tau_{r\theta}(r, \theta) = \eta \left( -\psi_{,rr} + \frac{1}{r} \psi_{,r} + \frac{1}{r^2} \psi_{,\theta\theta} \right) \quad (24)$$

The shear stress at  $\theta = 0$  (note that  $T_n(0) = 0$  because  $\psi_{,r} = 0$ ) which acts on the base of the lithosphere is

$$\tau_{r\theta}(r, 0) = \eta \left[ \frac{\alpha(\theta_0)}{r} + \sum_{n=2}^{\infty} a_{n-1} \beta_n(\theta_0) r^{n-2} \right] \quad (25)$$

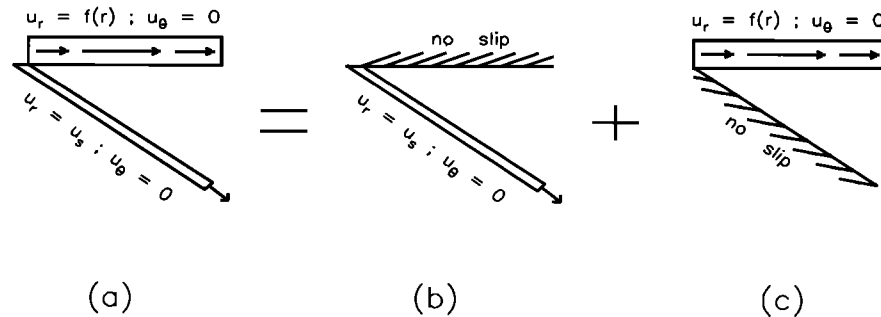


Fig. 2. (a) A schematic diagram showing the velocity boundary conditions for the corner flow model with a deformable overlying plate and a rigid subducting plate. (b) and (c) In case of a Newtonian fluid, the flow in the wedge can be separated into two simple corner flow models.

where  $\alpha$  and  $\beta_n$  are functions of the angle of subduction that are given by

$$\alpha(\theta_0) = \frac{2(\theta_0 \cos \theta_0 - \sin \theta_0)}{\theta_0^2 - \sin^2 \theta_0} \quad (26a)$$

$$\beta_n(\theta_0) = \frac{T_n''(0)}{T_n'(0)} \quad (26b)$$

$T_n'(0)$  and  $T_n''(0)$  are the first and second derivatives of  $T_n(\theta)$  at  $\theta = 0$ .

To evaluate  $\beta_n(\theta_0)$ , we solve (14), (15), and (16) using the following identities which are derived from the boundary conditions (equations (19a), and (20)):  $T_n(0) = T_n(\theta_0) = T_n'(\theta_0) = 0$ . This enables us to evaluate three of the four arbitrary constants in (14), (15), and (16). By substituting the first and second derivatives of  $T_n(\theta)$  into (26b), we eliminate the fourth arbitrary constant and get an expression that depends only on the angle of subduction. The solutions are

$$\beta_1(\theta_0) = 2 \frac{\theta_0 - \sin \theta_0 \cos \theta_0}{\sin^2 \theta_0 - \theta_0^2} \quad (27)$$

$$\beta_2(\theta_0) = \frac{2\theta_0 \cos 2\theta_0 - \sin 2\theta_0}{1 - \cos 2\theta_0 - \theta_0 \sin 2\theta_0} \quad (28)$$

For  $n > 2$ ,

$$\beta_n(\theta_0) = \frac{(4 - 4n)[(n - 2) \sin n\theta_0 \cos(n - 2)\theta_0 - (2n^2 - 4n)[1 - \cos n\theta_0 \cos(n - 2)\theta_0] - n \sin(n - 2)\theta_0 \cos n\theta_0}{(2n^2 - 4n + 4) \sin n\theta_0 \sin(n - 2)\theta_0} \quad (29)$$

Using the same characteristic parameters as in the thin viscous sheet model, the nondimensional shear traction on the base of the lithosphere becomes

$$T_{xz}^d = \gamma \left[ \frac{\alpha(\theta_0)}{x} + \sum_{n=0}^{\infty} a_{n+1} \beta_{n+2}(\theta_0) x^n \right] \quad (30)$$

where  $\gamma$  is the ratio of wedge viscosity to the overlying plate (thin sheet) viscosity. In the physical world  $\gamma$  is the ratio between asthenospheric viscosity ( $\eta_a$ ) and lithospheric viscosity ( $\eta_l$ ):

$$\gamma = \frac{\eta_a}{\eta_l} \quad (31)$$

The magnitude of the viscosity ratio determines the magnitude of the viscous forces in the asthenosphere, which are transmitted to the base of the lithosphere as shear traction.

The shear traction on the base of the lithosphere (equation (30)) is the sum of tractions from two processes. The first is the subduction of a rigid plate, and the other is the deformation of the overriding lithosphere. The shear traction arising from subduction contains a singularity at the origin. We assume that the lithosphere has a finite strength and that it yields under large shear stresses; thus, we limit the large traction near the origin ( $0 < x < x_1$ ) to a finite value. The modified shear traction that removes the singularity is

$$T_{xz}^d = \gamma \left[ \frac{\alpha(\theta_0)}{\hat{x}(x)} + \sum_{n=0}^{\infty} a_{n+1} \beta_{n+2}(\theta_0) x^n \right] \quad (32)$$

where

$$\hat{x}(x) = \begin{cases} x_1 & 0 < x < x_1 \\ x & x_1 < x < 1 \end{cases}$$

and  $x_1$  is small ( $x_1 \leq 0.1$ ). In the solutions below, we specify a value of  $x_1$ . In practice, the position of  $x_1$  is presumably determined by the yield strength of the lithosphere.

#### MODEL SOLUTIONS: INTERACTION BETWEEN THE THIN SHEET AND THE CORNER FLOW MODELS

In the thin viscous sheet model the deformation and velocity field within the lithosphere depends on basal drag (equation (10)). In turn, the shear traction on the base of the lithosphere from the corner flow model depends on the velocity field within the lithosphere (equation (32)). By substituting (32) into (10), we get an ordinary differential equation with one unknown: the velocity field in the deforming overlying plate. In this study we consider only simple models that allow analytical solutions. The simplest are those containing a Newtonian lithosphere with zero Argand number. The governing equation, in this case, is

$$\frac{d^2 u}{dx^2} = - \left( \frac{\gamma}{4L} \right) \left[ \frac{\alpha}{\hat{x}(x)} + \sum_{n=0}^{\infty} a_{n+1} \beta_{n+2} x^n \right] \quad (33)$$

where  $u$  is the velocity field of the lithosphere that is represented as a power series ( $u = \sum a_n x^n$ ),  $L$  is the dimensionless thickness of the lithosphere,  $\alpha$  and  $\beta_n$  are the shear traction coefficients which are functions of the angle of subduction (equations (26a), (27), (28), and (29)), and  $\gamma$  is the viscosity ratio (equation (31)). The boundary conditions are zero velocity at the wedge tip ( $u(0) = 0$ ), a finite velocity of the rigid plate far from the trench ( $u(1) = u_0$ ), and a constant subduction velocity which is used to scale the other velocities ( $u_s = 1$ ).

We use a perturbation method to solve the equations for the velocity and the strain rate fields with  $\frac{\gamma}{4L}$  as the small parameter. We have few constraints on the viscosity ratio ( $\gamma$ ) and on the dimensionless thickness of the lithosphere ( $L$ ). However, by using the single ratio  $\frac{\gamma}{4L}$  as the small parameter, we reduce the number of free parameters and hence the uncertainties somewhat. Generally, the thickness of the lithosphere is in the range 50–100 km, and the width of the zone of deformation (the characteristic length scale  $D$ ) is in the range of 400–1000 km. Thus, a typical value for the dimensionless thickness of lithosphere above subduction zones is  $L \sim \frac{1}{10}$ . The viscosity ratio is very small ( $\gamma \ll \frac{1}{10}$ ); hence, the range of the small parameter is  $0 \leq \frac{\gamma}{4L} \leq \frac{1}{4}$ .

The solution without perturbation corresponds to a lithosphere that overlies an inviscid asthenosphere ( $\gamma = 0$ ). The governing equation (33) reduces to

$$\frac{d^2 u}{dx^2} = 0 \quad (34)$$

We use the boundary conditions from above ( $u(0) = 0$ ;  $u(1) = u_0$ ) to get

$$u = u_0 x \quad (35a)$$

$$\frac{du}{dx} = u_0 \quad (35b)$$

This solution represents homogeneous or uniform deformation and describes the deformation of the lithosphere without any influence from the asthenosphere below. Extension occurs when  $u_0 > 0$ , with positive horizontal and negative vertical strain rates. Compression occurs when  $u_0 < 0$ , with negative horizontal and positive vertical strain rates.

Since the boundary conditions are already satisfied, any perturbation should satisfy zero velocities at both ends of the deformed lithosphere ( $\tilde{u}(0) = \tilde{u}(1) = 0$ ). The unperturbed solution ( $u = u_0x$ ) causes constant shear traction on the base of the lithosphere in the direction opposite to the motion of the lithosphere. The only nonzero coefficient of the lithospheric velocity is  $a_1 = u_0$ , and the shear traction due to this term is  $u_0\beta_2$  (equation (33)). The governing equation for the first-order perturbation is

$$\frac{d^2\tilde{u}}{dx^2} = -\left(\frac{\gamma}{4L}\right) \left[ \frac{\alpha(\theta_0)}{\hat{x}(x)} + u_0\beta_2(\theta_0) \right] \tag{36}$$

where  $\alpha/\hat{x}(x)$  represents traction from the subduction of a rigid plate and  $u_0\beta_2$  represents traction from viscous resistance to the uniform deformation of the lithosphere. We solve (36) with the zero-velocity boundary conditions ( $\tilde{u}(0) = \tilde{u}(1) = 0$ ). The solution for the velocity field is

$$u = u_0x + u_0\beta_2 \left(\frac{\gamma}{4L}\right) \left[ \frac{x}{2}(1-x) \right] - \alpha \left(\frac{\gamma}{4L}\right) \begin{cases} \frac{x^2}{2x_1} + x(\log x_1 - \frac{x_1}{2}) & 0 < x < x_1 \\ \frac{x_1}{2} + x(\log x - \frac{x_1}{2}) & x_1 < x < 1 \end{cases} \tag{37}$$

and for the strain rate field is

$$\frac{du}{dx} = u_0 + u_0\beta_2 \left(\frac{\gamma}{4L}\right) \left[ \frac{1}{2} - x \right] - \alpha \left(\frac{\gamma}{4L}\right) \begin{cases} \frac{x}{x_1} + \log x_1 - \frac{x_1}{2} & 0 < x < x_1 \\ 1 + \log x - \frac{x_1}{2} & x_1 < x < 1 \end{cases} \tag{38}$$

This first-order perturbation of the deformation is due to the subduction of the rigid plate and the viscous resistance to the uniform deformation. The second-order perturbation arises from viscous resistance to the first-order velocity perturbation. Since the perturbed velocities are small (of the order of  $(\frac{\gamma}{4L})$ ), the second-order perturbation of the deformation is very small (of the order of  $(\frac{\gamma}{4L})^2$ ), and we therefore will neglect it.

The total deformation (equations (37) and (38)) is a result of three simultaneous processes: uniform deformation due to horizontal force acting on the plate boundaries, viscous resistance to the uniform deformation, and traction resulting from subduction of a rigid plate. The horizontal force acting on the plate boundaries dominates the nature of the deformation. Large-scale compression occurs when the trench moves toward the rigid lithosphere ( $u_0 < 0$ ), and large-scale extension occurs when the trench moves away from the rigid lithosphere ( $u_0 > 0$ ) (Figure 1). Local variations in the magnitude of the deformation may result from shear tractions acting on the base of the lithosphere. If those tractions are large enough, the nature of the deformation can change locally from compressional to extensional or vice versa.

We demonstrate the case of large-scale compression ( $u_0 < 0$ ) by using a solution with a particular set of parameters and boundary conditions ( $\theta_0 = 45^\circ$ ;  $\frac{\gamma}{4L} = 0.2$ ;  $u_0 = -0.4$ ) (Figure 3a). The unperturbed solution is a uniform com-

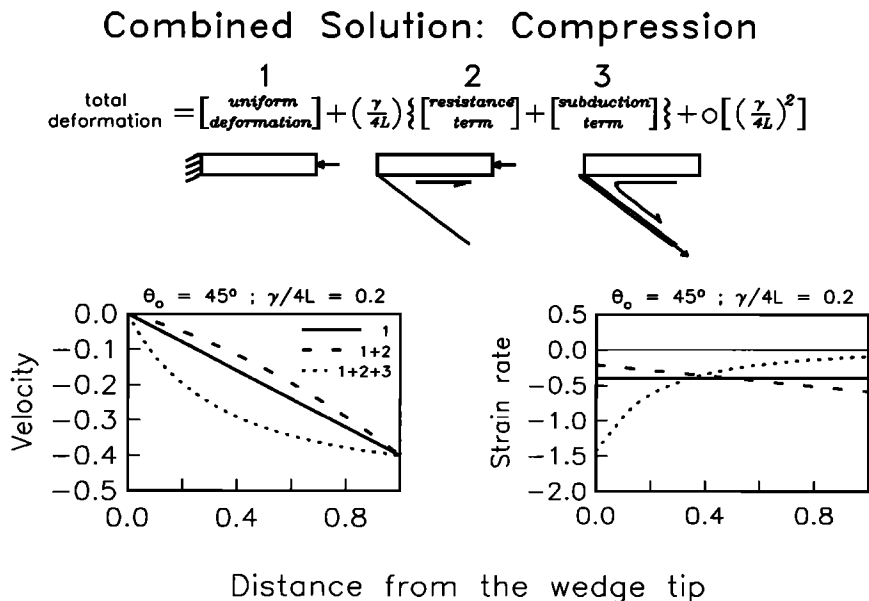


Fig. 3a. Cumulative solutions of velocity and strain rate fields for large-scale compressional environments ( $\theta_0 = 45^\circ$ ;  $\frac{\gamma}{4L} = 0.2$ ;  $u_0 = -0.4$ ). For the uniform deformation solution (solid line) we add the first-order perturbation of magnitude  $\frac{\gamma}{4L}$ . First the deformation resulting from viscous resistance to the uniform deformation is added to the uniform deformation (dashed line). Second, the deformation resulting from subduction of a rigid plate is added to the uniform and the resistance deformation (dotted curve).

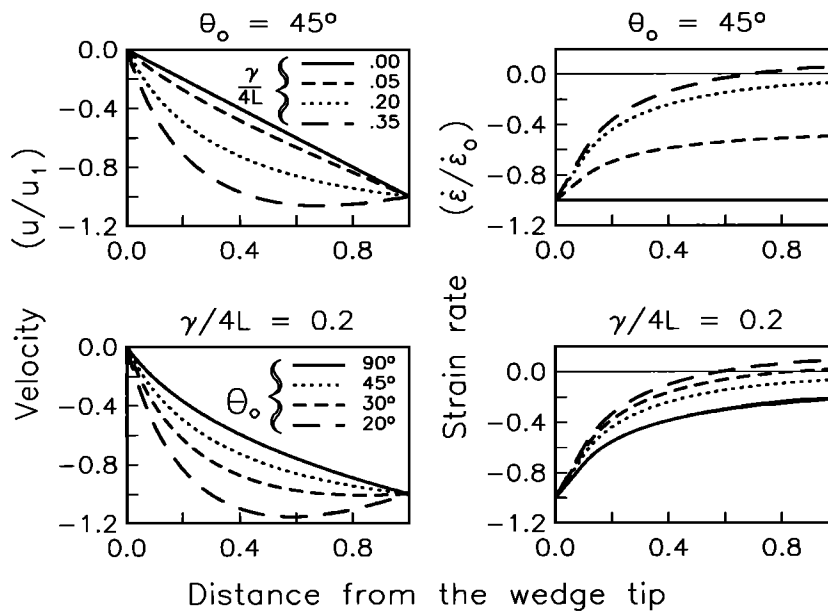


Fig. 3b. Velocity and strain rate solutions for large-scale compressional environments ( $\theta_0 = 45^\circ$ ;  $\frac{\gamma}{4L} = 0.2$ ;  $u_0 = -0.4$ ) showing the sensitivity of the solutions to variations in (top)  $\frac{\gamma}{4L}$  and (bottom)  $\theta_0$ . The velocities are scaled by the velocity at the far field ( $u_1 = |u(1)|$ ), and the strain rates are scaled by the strain rate at the wedge tip ( $\dot{\epsilon}_0 = |\dot{\epsilon}(0)|$ ).

pressional strain rate (solid line). The addition of the drag arising from resistance to uniform compression (dashed line) decreases the compressional strain rate near the wedge tip and increases it farther away. The contribution of the drag from subduction increases the compressional strain rate near the wedge tip and reduces it farther away (dotted curve), which is opposite to the effect of the drag from resistance to uniform compression. When the magnitude of the velocity boundary condition is sufficiently small ( $-0.5 < u_0 < 0$ ), the subduction term is dominant near the wedge tip, but farther away the two terms tend to cancel each other. Thus, most of the deforming lithosphere is subjected to a moderate compression, except the region near the wedge tip where the compression is more intense. The solution also depends on the choice of the parameters  $\theta_0$  and  $\frac{\gamma}{4L}$ . When  $\theta_0$  is fixed, the deviation of the total deformation from that with uniform compression increases with  $\frac{\gamma}{4L}$  (Figure 3b, top). When  $\frac{\gamma}{4L}$  is fixed, the deviation of the total deformation departs more from uniform compression as  $\theta_0$  decreases (shallower angle of subduction) (Figure 3b, bottom). For increasing values of  $\frac{\gamma}{4L}$ , or a shallower angle of subduction, the strain rate field decays faster with distance from the wedge tip. For large values of  $\frac{\gamma}{4L}$ , or for a shallow subduction, the zone of compressional strain rate exists only in a finite zone next to the wedge tip, while a zone of an extensional strain rate exists farther away. Thus, the broad zone of moderate compression that exists with low values of  $\frac{\gamma}{4L}$ , or with steep angle of subduction, will tend to get narrower if  $\frac{\gamma}{4L}$  is increased or the angle of subduction is decreased.

We use the same analysis to demonstrate the effect of shear traction on large-scale extension ( $u_0 > 0$ ) by choosing  $\theta_0 = 60^\circ$ ,  $\frac{\gamma}{4L} = 0.2$ , and  $u_0 = 0.9$  (Figure 4a). In large scale extension the resistance and the subductions terms add and amplify the local deformation. For increasing values of  $\frac{\gamma}{4L}$ , or a shallower angle of subduction, the strain rates decay

faster from the far field toward the wedge tip (Figure 4b). For large values of  $\frac{\gamma}{4L}$ , or for a shallower subduction, a zone of compressional strain rate may exist near the wedge tip, while most of the lithosphere is subjected to extension.

For both large-scale compression and extension, the sum of the shear tractions acting on the base of the lithosphere is directed toward the wedge tip. Since variations in  $\theta_0$  influence mostly the magnitude and only slightly the distribution of the shear tractions (equation (36)), the sensitivity of the solutions for variations in  $\theta_0$  is similar to that for variations in  $\frac{\gamma}{4L}$ . For increasing values of  $\frac{\gamma}{4L}$ , or for a shallower angle of subduction, the total tractions acting on the base of the lithosphere increase and are directed toward the wedge tip. As a result, the region near the wedge tip is subjected to more compression (or less extension), and the region far from the wedge tip is subjected to more extension (or less compression).

The analytical solutions of the simple models discussed above give insight into deformation above subduction zones. They allow us to identify the important processes that affect deformation. The deformation of the lithosphere is dominated by horizontal force acting on its plate boundary and is affected by basal shear traction. The major contributors to shear traction are the subduction of a rigid plate and the viscous resistance of the asthenosphere to the uniform deformation. The identification of the various sources of shear traction is useful for calculations with nonlinear rheology, in which the different processes may not be so easily separated.

## DISCUSSION

We now apply this simple model to two situations: compressional (the Andes) and extensional (the Aegean). Our aim is to find parameters for which the model may produce geologically interesting results. We shall see that the model

Combined Solution: Extension

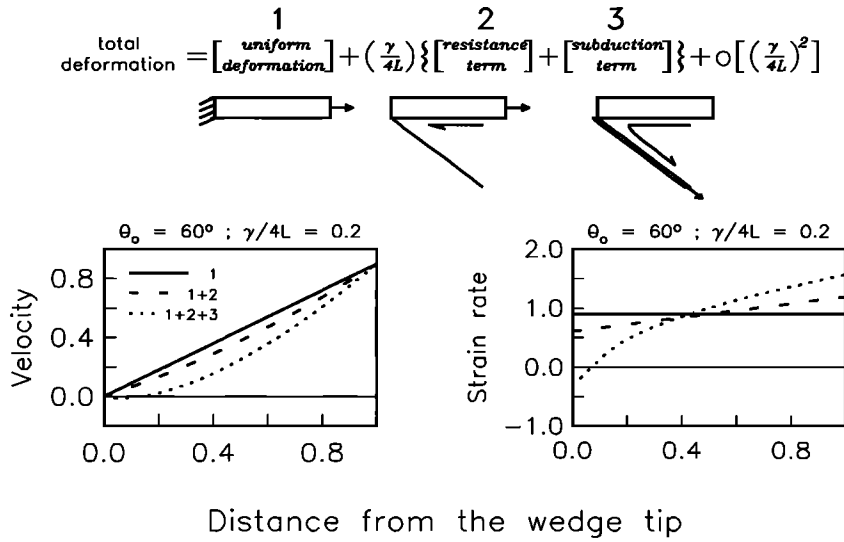


Fig. 4a. Cumulative solutions of velocity and strain rate fields for large-scale extensional environments ( $\theta_0 = 60^\circ$ ;  $\frac{\gamma}{4L} = 0.2$ ;  $u_0 = 0.9$ ) as in Figure 3a.

explains some of the features of the deformation in both areas that have not been explained by previous models. We are not, however, trying to demonstrate that every feature observed in the Aegean or the Andes is predicted by our calculations.

The solutions for the velocity and strain rate fields (equations (37) and (38)) depend on characteristic parameters and on the velocity boundary condition that must be specified a priori. The trench velocity ( $u_t$ ) and the subduction velocity ( $u_s$ ) are found from global and local plate motion

models. The subduction velocity ( $u_s$ ) is the characteristic velocity used for scaling; thus, the dimensionless velocity boundary condition is  $u_0 = u_t/u_s$ . The shear traction coefficients  $\alpha(\theta_0)$  and  $\beta_n(\theta_0)$  depend on the angle of subduction which can be inferred from the distribution of seismic events. Benioff zone geometries do not always show the straight subducting slabs that we use in our model, but we estimate an angle for the best fit straight slab to within  $\pm 5^\circ$ . The dimensionless thickness of the lithosphere ( $L$ ) can be evaluated from the real thickness (50–100 km) divided

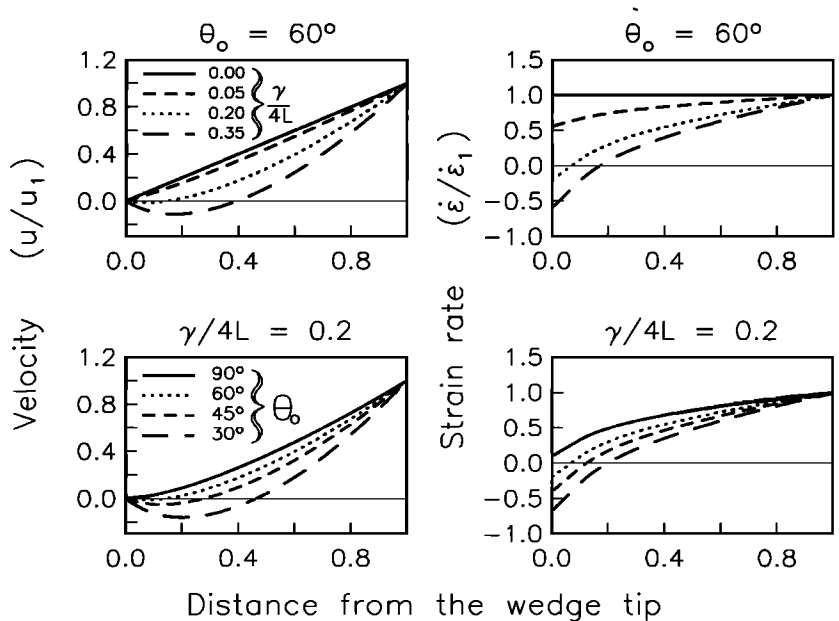


Fig. 4b. Velocity and strain rate solutions for large-scale extensional environments ( $\theta_0 = 45^\circ$ ;  $\frac{\gamma}{4L} = 0.2$ ;  $u_0 = -0.4$ ) showing the sensitivity of the solutions to variations in (top)  $\frac{\gamma}{4L}$  and (bottom)  $\theta_0$ . The velocities are scaled by the velocity at the far field ( $u_1 = |u(1)|$ ), and the strain rates are scaled by the strain rate at the far field ( $\dot{\epsilon}_1 = |\dot{\epsilon}(1)|$ ).

by the characteristic length scale (400–1000 km). A typical value for  $L$  above subduction zones is  $\frac{1}{10}$ ; therefore our thin sheet approximation should be accurate to 5–10% (see the appendix).

The last parameter to evaluate is the viscosity ratio ( $\gamma$ ), which is poorly constrained. Estimates of asthenospheric viscosity from postglacial rebound have assumed a linear rheology and have obtained an average viscosity of  $\sim 10^{21}$  Pa s [Cathles, 1975; Peltier and Andrews, 1976]. However, the uppermost asthenosphere may have a lower effective viscosity of  $\sim 4 \times 10^{19}$  Pa s [Walcott, 1973; Cathles, 1975]. Estimates of lithospheric viscosity have even fewer constraints. The effective viscosity of oceanic and continental (shield) lithosphere has been estimated to be  $10^{23}$ – $10^{24}$  Pa s from the flexural response to long-term loads [Walcott, 1970]; however, the viscosity of young continental crust is poorly determined. The effective viscosity of actively deforming regions may be estimated from a knowledge of their strain rates and of the likely range of vertically averaged stresses acting upon them. England and Houseman [1986] estimate the viscosity of the Asian lithosphere to be about  $0.5$ – $1.0 \times 10^{24}$  Pa s, while England [1986] argues that the average viscosity of the lithosphere might need to be as low as  $10^{22}$  Pa s for extensional regions to deform as rapidly as they do. The above viscosity estimates suggest that the ratio of asthenospheric to lithospheric viscosity is  $4 \times 10^{-5} < \gamma < 0.10$  and that  $10^{-4} < \frac{\gamma}{4L} < 0.25$ . The results illustrated in Figures 3 and 4 show that the influence of basal shear stresses on the tectonics of the overriding plate is appreciable only if  $\frac{\gamma}{4L} > 0.01$ , so a large part of the range of possible values of  $\frac{\gamma}{4L}$  is unlikely to produce geologically interesting effects.

In each of the cases illustrated in Figures 3 and 4, the influence of the circulation in the asthenospheric wedge is to make the strain rate in the lithosphere near the tip of the wedge more compressional and to make strain rates far from the tip more extensional. In the next two sections we look at the tectonics of two regions, the Andes and the Aegean, to see if they show styles of deformation consistent with basal shear tractions applied by flow in the asthenosphere and to attempt to bound the value of  $\frac{\gamma}{4L}$  in these regions.

#### The Andes: Compressional Tectonics

The formation of the Andes mountain belt is associated with the subduction of the Nazca plate beneath western South America. Indeed, this type of tectonic environment of mountain belt above a subduction zone is frequently called an Andean-type margin [Dewey and Bird, 1970]. The topography of the central Andes ( $5^{\circ}$ – $34^{\circ}$ S) can be divided into three segments which coincide with the segmentation of the subducting Nazca plate (Figure 5). The central segment ( $15^{\circ}$ – $27^{\circ}$ S), where the angle of subduction is relatively steep ( $30^{\circ}$ ) [Stauder, 1975; Barazangi and Isacks, 1976], is characterized by the broad Altiplano Plateau (B-B' in Figure 5b). The plateau relief is moderate with an elevation of 3.5–4.5 km above sea level and a width of about 800 km. The northern segment ( $5^{\circ}$ – $15^{\circ}$ S) (A-A' in Figure 5b) and the southern segment ( $27^{\circ}$ – $34^{\circ}$ S) (C-C' in Figure 5b) where the angle of subduction is very shallow ( $10^{\circ}$ – $15^{\circ}$ ) [Stauder, 1975; Barazangi and Isacks, 1976] are characterized by a narrower zone of elevated topography. The average elevation of the Andes at these segments is greater than 3.0 km

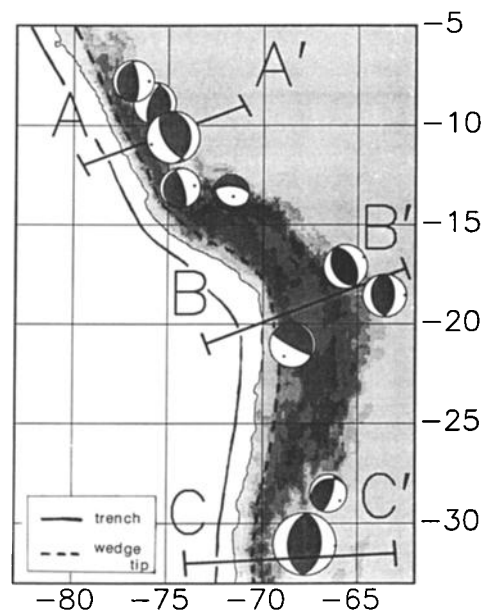


Fig. 5a. Seismic activity in the Andes in the years 1977–1987 ( $M_W > 5.0$ ; radius is proportional to  $M_W$ ). ( $M_W$  is determined from digital seismograms of the Global Digital Seismic Network (GDSN), using the centroid moment tensor (CMT) method described by Dziewonski et al. [1981] and Dziewonski and Woodhouse [1983].)

above sea level, with peaks that reach more than 6.0 km, and the width of the mountain belt is in the range of 200–400 km. The high topography of the region is supported by thick crust with an average thickness of 60 km [James, 1971], and possibly by thermally thinned lithosphere underlain by low-density asthenosphere [Froidevaux and Isacks, 1984]. The seismic deformation within the Andes belt is concentrated along the eastern and western flanks of the mountain belt, beneath areas of low topographic elevation [Suárez et al., 1983; Isacks, 1988] (also see the centroid moment tensor (CMT) solutions in Figure 5a). Fault plane solutions show mostly thrust faulting with the  $P$  axis oriented approximately perpendicular to the mountain chain. Suárez et al. [1983] estimate the seismic strain rate of the eastern part of the northern and central segments as  $2 \times 10^{-16} \text{ s}^{-1}$  ( $6.3 \times 10^{-9} \text{ yr}^{-1}$ ). Extension (normal faulting) observed in the high Andes is attributed to buoyancy forces due to high mountains and their crustal root [Dalmayrac and Molnar, 1981].

We take the characteristic length scale ( $D$ ) as 800 km, the distance across the Altiplano in the central segment, which is the distance from the tip of the asthenospheric wedge (about 50 km inland from the coastline, Figure 5a) to the eastern slope of the Andes (B-B' in Figure 5b). The angle of subduction ( $\theta_0$ ) is  $30^{\circ}$  for the central segment and  $10^{\circ}$ – $15^{\circ}$  for the northern and southern segments. The thickness of the lithosphere is estimated as 80 km [Smalley and Isacks, 1987; Isacks, 1988]. Thus for the central segment the dimensionless thickness is  $L \sim \frac{1}{10}$ , which implies that our approximate solution is accurate to 5–10%. However, in the northern and southern segments the width of the deformed area is much narrower ( $\sim 400$  km) and as a result  $L \sim \frac{1}{5}$ . Since our model solution assumes  $L \ll 1$ , this may limit the accuracy of the results (see the appendix). Using the values discussed above

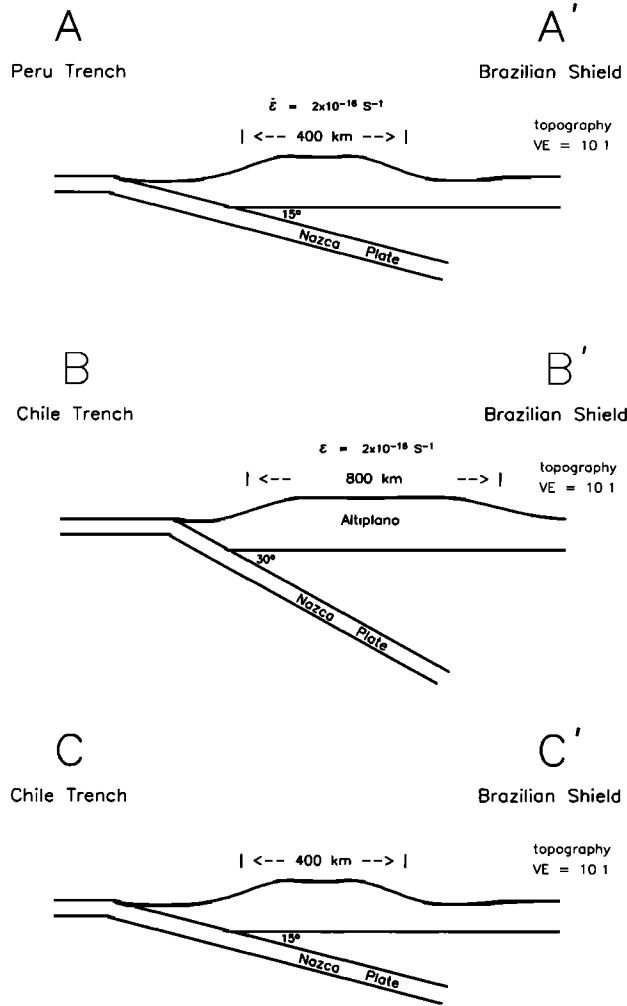


Fig. 5b. Schematic cross sections the Andes, in E-W direction; A-A' is across the northern segment; B-B' is across the central segment; and C-C' is across the southern segment. The strain rate  $\dot{\epsilon}$  is from Suárez *et al.* [1983].

for the viscosity ratio ( $10^{-4} < \gamma < 0.05$ ), the range of the small parameter we use is  $0 \leq \frac{\gamma}{4L} \leq \frac{1}{10}$ . The subduction velocity ( $u_s$ ) is usually taken as the convergence velocity between the Nazca and the South American plates, about  $100 \text{ mm yr}^{-1}$  [Chase, 1978; Munster and Jordan, 1978]. However, the velocity between the trench and the rigid plate ( $u_t$ ) is poorly known. Estimates for the trench velocity fall in the range  $2\text{--}10 \text{ mm yr}^{-1}$  [Suárez *et al.*, 1983; Isacks, 1988; Roeder, 1988]. We assume that the South American plate is moving westward at  $100 \text{ mm yr}^{-1}$  with respect to the Nazca plate and that the trench is moving eastward in velocity  $u_t$  with respect to South America. Thus, the velocity of the Nazca plate with respect to the trench, which is the subduction velocity ( $u_s$ ), is the difference between the two velocities ( $u_s = 100 - u_t$ ).

Because we arbitrarily impose a width on our deforming zone (Figure 1) we have essentially fixed the scale of the strain rate once we have chosen the velocity of the trench ( $u_t$ ). According to our choice of parameters (Table 1), the lithospheric strain rate is scaled to the order of  $10^{-16} \text{ s}^{-1}$ . We cannot, therefore, use estimates of strain rates in the Andes [e.g., Suárez *et al.*, 1983] to estimate the values of

TABLE 1. Values of Parameters Used in Calculations for the Andes and the Aegean

Description	Andes	Aegean	
$D$	length scale, km	800	600
$\theta_0$	angle of subduction	$10^\circ\text{--}30^\circ$	$35^\circ$
$u_s$	subduction velocity	90–98	30–80
$u_t$	trench velocity	(-10)–(-2)	20–70
$\gamma$	viscosity ratio, $\eta_a/\eta_l$	0–0.02	0–0.1
$L$	dimensionless thickness	0.1	0.1
$\frac{\gamma}{4L}$	the small parameter	0.0–0.05	0.0–0.25

Velocities in  $\text{mm yr}^{-1}$

our calculations. However, the observations of tectonic style do impose one important constraint: there is horizontal compression to the east of the Andes, and therefore any shear traction acting on the base of the lithosphere must not outweigh the overall compression applied by the boundary conditions.

In the configuration of our calculations (Figure 3b) the sign of the strain rate at great distance from the wedge tip depends on the small parameters ( $\frac{\gamma}{4L}$ ) and upon the dip of the subducting slab ( $\theta_0$ ). Figure 6 shows the range of values of  $\frac{\gamma}{4L}$  and  $\theta_0$  that yield net compression far from the wedge tip for  $u_t$  in the range  $2\text{--}15 \text{ mm yr}^{-1}$ . Thus we conclude that the basal shear tractions owing to circulation in the asthenospheric wedge beneath the central segment of the Andes ( $\theta_0 = 30^\circ$ ) will not result in net extension in the overriding plate provided that  $0 < \frac{\gamma}{4L} < 0.025$  for the estimated values of  $u_t$  ( $2\text{--}10 \text{ mm yr}^{-1}$ ).

The major features of deformation in the Andes that are not reproduced by our analysis are the low rate of seismic activity in the western Andes and low (probably mainly extensional) strain rate in the high Andes. Although, our analysis omits buoyancy forces (equation (10)), we can suggest the role that buoyancy might play from the following simple argument based on (8). The influence of the buoyancy alone may be expressed as

$$\frac{d^2 u}{dx^2} = \frac{Ar}{4L} \frac{d(S^2)}{dx} \quad (39)$$

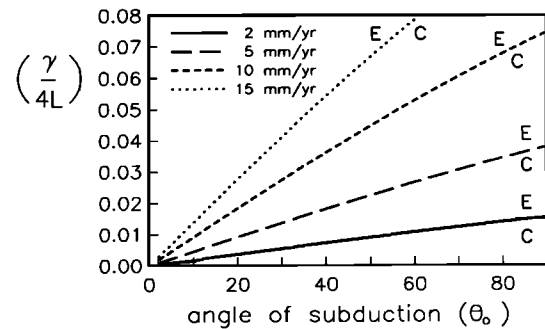


Fig. 6. Range of  $\frac{\gamma}{4L}$  and  $\theta_0$  for which extensional strain rate occurs in the overriding plate ( $D = 800 \text{ km}$ , and  $u_t$  is varied between  $2$  and  $15 \text{ mm yr}^{-1}$ ). The lines separate parameter ranges in which extension (E) occurs far from the wedge tip in the overriding plate from parameter ranges in which the overriding plate is always in compression (C).

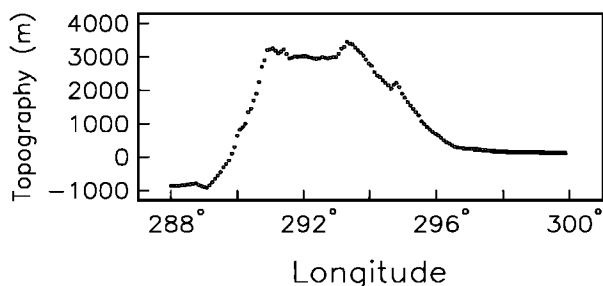


Fig. 7. An E-W topography section through the Andes from 72°W to 60°W obtained by averaging the topography in a swath of a latitude 4° wide, centered on 20°S.

This is (8) neglecting basal tractions. Thus, if we specify the form of the crustal thickness variations, we may estimate the contribution to the strain rate field from the buoyancy forces and add it to the strain rate field we have calculated by neglecting buoyancy. This approach does not, of course, explain the form of the topography which could only be determined by a full, time-dependent solution that is beyond the scope of this paper.

From (39) the form of the strain rate due to buoyancy forces is

$$\frac{du}{dx} = \frac{Ar}{4L} (S^2 - S_0^2) \quad (40)$$

The quantity  $(S^2 - S_0^2)$  may be estimated from a knowledge of the topography by assuming Airy isostatic equilibrium and values for the density of crust and mantle and of the crustal thickness  $S_0$  for zero surface height. Figure 7 shows this quantity for an E-W transect through the Andes from 72°W to 60°W obtained by averaging the topography in a swath of a latitude 4° wide, centered on 20°S.

Figure 8 illustrates, schematically, the result of superimposing a strain rate due to the buoyancy of the Andean topography (8a) upon the strain rates due to the boundary value problem discussed here (8b). If the maximum extensional strain rates owing to buoyancy are of the same order as those due to the boundary conditions, the combined strain rate field (8c) shows much reduced compression near the trench, extension in the Andes, and compression to the west of the Andes. This is in qualitative agreement with the observed strain rate field.

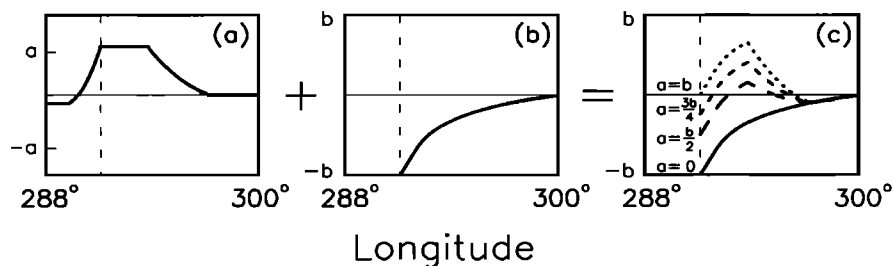


Fig. 8. A schematic illustration of the contribution of buoyancy forces on the overall deformation in the Andes showing (a) strain rate due to buoyancy estimated from the topography (Figure 7) by assuming Airy isostatic equilibrium (scaled to  $a$ ), (b) strain rate due to boundary value problem (scaled to  $b$ ), and (c) summed strain rate for various ratios of  $a$  and  $b$ . The buoyancy forces tend to decrease the compression in the western and the high Andes. If the buoyancy forces are sufficiently large ( $a \geq b/2$ ), extensional strain rate will occur in the high Andes.

*The Effect of the Angle of Subduction on the Deformation*

In the different segments of the central Andes, different angles of subduction correlate with the width of the zone of deformation in the overlying plate [Stauder, 1975; Barazangi and Isacks, 1976]. The foregoing discussion covered only the central segment where the uplifted plateau is very broad. Another characteristic feature of the deformation illustrated in Figure 3 is that the shear traction on the base of the lithosphere exerts a control on the width of the zone of appreciable compressional deformation (Figure 3b). If  $\frac{\gamma}{4L}$  is fixed, then the width of the zone of compression is determined by the dip of the subduction zone. To illustrate this point, we use the following set of parameters and boundary conditions that matches the observations the best ( $\frac{\gamma}{4L} = 0.02$ ;  $u_t = -10 \text{ mm yr}^{-1}$ ;  $u_s = 90 \text{ mm yr}^{-1}$ ) and vary the angle of subduction ( $\theta_0$ ). Figure 9 illustrates the solutions of the model where the free parameter is the angle of subduction. It shows that above a shallow-dipping slab the strain rate field decays faster than above a steep-dipping slab. For a 30° dipping slab, the zone of compression and uplift extends over the entire 800 km. However, for 10° and 15° dipping slabs, the zones of compression extend only 450 and 550 km from the wedge tip, respectively. According to our model, the horizontal extent of uplifted topography, which is supported by compressional stresses, depends on the angle of subduction. A wide zone of uplifted topography (plateau) tends to develop above a relatively steeply dipping slab, whereas a narrower zone (mountain chain) would develop above a more shallowly dipping slab.

The overall compression is caused by horizontal forces that push the Brazilian Shield toward the trench where the Nazca plate is subducting. The subduction of a rigid plate, as well as the compression of the lithosphere, produces an asthenospheric flow in the wedge underneath the Andes, which shears the base of the lithosphere toward the tip of the wedge. This increases the compression near the trench and decreases it farther away. For shallow subduction, the magnitudes of the shear tractions acting on the base of the lithosphere are larger, causing more lithospheric material to move toward the wedge tip. A zone of intense compression tends to develop next to the wedge tip, which reduces the compression (and may in some cases cause extension) farther from the wedge tip. Thus, the width of the zone of compression is narrower for the case of shallow subduction. These results are in agreement with the observations of the three segments of the central Andes. In the central segment, where

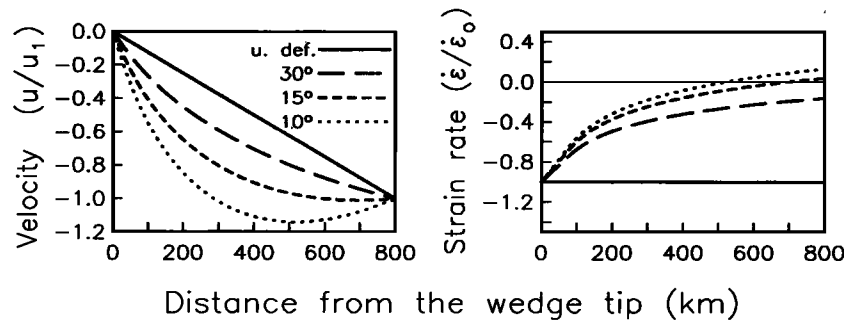


Fig. 9. Solutions for the boundary conditions for the Andes with various values of angle of subduction ( $\frac{\gamma}{4L} = 0.02$  and  $u_t = -10 \text{ mm yr}^{-1}$ ). The velocities are scaled by the velocity at the far field ( $u_1 = |u(1)|$ ), and the strain rates are scaled by the strain rate at the wedge tip ( $\dot{\epsilon}_0 = |\dot{\epsilon}(0)|$ ). The uniform deformation solution (solid line) is independent of angle of subduction. The zone of compression for  $\theta_0 = 30^\circ$  (central segment) extends to the entire 800 km; however, for  $\theta_0 = 10^\circ$  and  $15^\circ$  (southern and northern segments) the zone of compression extends only 450–550 km. Buoyancy forces are not included in the calculations; see Figure 8.

the Nazca plate dips at  $30^\circ$ , the uplifted topography, which is supported by compressional stresses, is the widest. In the northern and southern segments, where the subduction is shallower ( $10^\circ$ – $15^\circ$ ), the uplifted topography is restricted to a narrower zone.

Many studies [e.g., Hamilton, 1969; Burchfiel and Davis, 1975] suggest that the Mesozoic Cordilleran orogenic belt of the western United States is an older and deeply eroded Andean-type mountain belt. Bird [1984, 1988] argues that the formation of the Mesozoic Rocky Mountains results from a shearing of the western North America plate by the horizontally subducted Farallon plate. However, the observations from the Andes show that the widest mountain structure develops above a thick asthenospheric wedge that is bounded by a relatively steep-dipping slab ( $30^\circ$ ) and not above the near-horizontal slab. Therefore, we suggest that, if the western United States indeed deformed during the Mesozoic similar to the present-day deformation of the Andes, the cause was horizontal shortening resulting from the motion of the North American plate toward the trench offshore the Pacific coast above an asthenospheric wedge. In such a case, the Farallon plate may well have been subducted at a relatively steep angle ( $\sim 30^\circ$ ) and not horizontally as suggested by Bird [1984, 1988].

#### The Aegean: Extensional Tectonics

The subduction of the African plate under the Eurasian plate along the Hellenic arc is the most-studied example of large-scale extension of continental lithosphere above a subduction zone. The extensive seismicity of the Aegean (Figure 10a) indicates that most of the area extends by normal and strike-slip faulting except for a narrow belt of compressional thrust faults along the arc. The extension began at 13 Ma [Le Pichon and Angelier, 1979] or possibly at 5 Ma [Jackson and McKenzie, 1988] and has reached up to 65% [Le Pichon and Angelier, 1981]. The Aegean extension is predominantly directed N-S, subparallel to the direction of convergence between Africa and Eurasia. Most of the seismic extension is concentrated in an area of  $500 \times 500 \text{ km}^2$  in the northern Aegean, while the southern Aegean, which contains the thinnest crust, is relatively inactive [McKenzie, 1978; Jackson and McKenzie, 1988] (also see the centroid moment tensor (CMT) solutions in Figure 10a). Jack-

son and McKenzie [1988] calculate an average seismic strain rate of  $4 \times 10^{-15} \text{ s}^{-1}$  in the N-S direction for the northern Aegean (400–600 km from the wedge tip); however, Ekström and England [1989] suggest the above value may be too large by about a factor of 3. Given the uncertainties, we use the above values as upper and lower bounds for the strain rate  $1.5 \times 10^{-15} \text{ s}^{-1} < \dot{\epsilon} < 4.0 \times 10^{-15} \text{ s}^{-1}$  ( $4.7 \times 10^{-8} \text{ yr}^{-1} < \dot{\epsilon} < 1.25 \times 10^{-7} \text{ yr}^{-1}$ ). The zone of compression has an arc shape and extends up to 100 km from the trench. Figure 10b shows a schematic cross section of the Aegean in a N-S direction that illustrates the available observations.

We take the characteristic length scale ( $D$ ) as 600 km, the distance from the tip of the asthenospheric wedge (approximately underneath Crete, Figure 10a) to the undeformed continental lithosphere (approximately northern Greece). From the geometry of the Benioff zone we choose an angle of subduction ( $\theta_0$ ) of  $35^\circ$  [Papazachos, 1973; McKenzie, 1978]. The dimensionless thickness of the lithosphere ( $L$ ) is poorly known; we estimate  $L \sim \frac{1}{10}$ . Our solution depends principally on the ratio  $\frac{\gamma}{4L}$ , which is the small parameter in

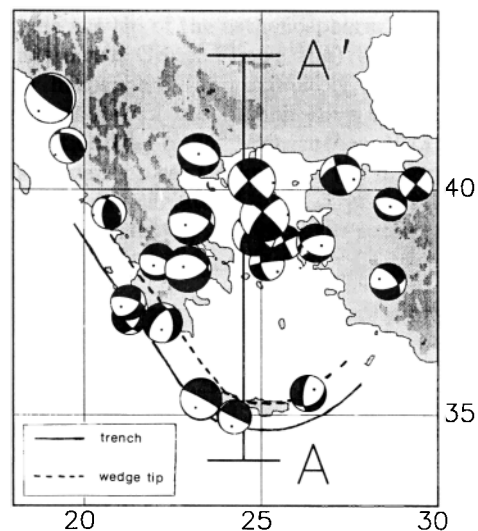


Fig. 10a. Seismic activity in the Aegean in the years 1977–1987 ( $M_W > 5.0$ ; radius is proportional to  $M_W$ ) (determination of  $M_W$  is as explained in Figure 5a).

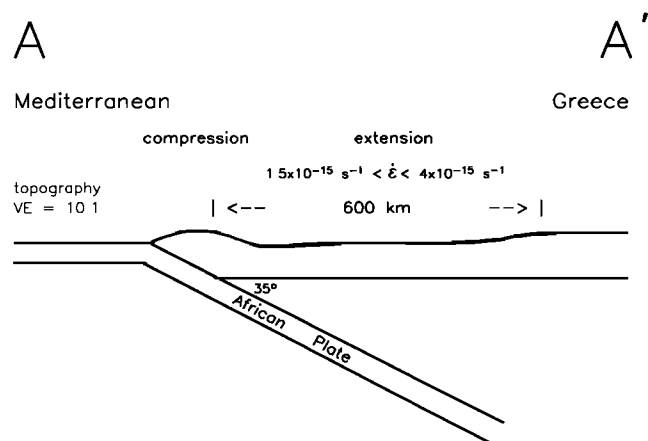


Fig. 10b. Schematic section across the Aegean, in N-S direction. The seismic strain rate  $\dot{\epsilon}$  from Jackson and McKenzie [1988] and Ekström and England [1988].

the perturbation; we use  $0 < \frac{\gamma}{4L} < \frac{1}{4}$ . The velocity between the trench and the rigid plate ( $u_t$ ) and subduction velocity ( $u_s$ ) are also poorly known. Estimates for the trench velocity are in the range 20–70 mm yr<sup>-1</sup> [McKenzie, 1978; Le Pichon and Angelier 1981; Jackson and McKenzie, 1988; Ekström and England, 1989]. Estimates for the subduction velocity follow directly from  $u_t$ , once the relative velocity between Africa and Eurasia is known. Global plate velocity models indicate convergence rate of 10 mm yr<sup>-1</sup> [Chase, 1978; Minster and Jordan, 1978]. We assume that Africa is moving 10 mm yr<sup>-1</sup> northward with respect to Eurasia, and the trench is migrating southward with velocity  $u_t$ , also with respect to Eurasia. Thus, the velocity of Africa with respect to the trench, which is the subduction velocity ( $u_s$ ), is the sum of the two velocities ( $u_s = u_t + 10 \text{ mm yr}^{-1}$ ).

With  $\theta_0$  fixed, the strain rate is determined by the value of  $\frac{\gamma}{4L}$  and the velocity boundary condition ( $u_0 = u_t/u_s$ ). Figure 11 shows contours of extensional strain rate at a distance of 500 km from the trench calculated for different values of  $\frac{\gamma}{4L}$  and  $u_t$  with the values of  $D$ ,  $L$ , and  $\theta_0$  given in Table 1. It can be seen that a strain rate comparable with those measured seismically can be obtained for a fairly wide range of  $u_t$ . When  $\frac{\gamma}{4L}$  is very small, then the strain rate is simply ( $u_t/D$ ) throughout the deforming region. An additional constraint is implied by the existence of a narrow zone of compression near the trench. If the origin of this lies in the asthenospheric flow, then Figures 11 and 12 show that  $\frac{\gamma}{4L}$  is in the range ( $0.08 < \frac{\gamma}{4L} < 0.15$ ) in order for there to be a narrow ( $\leq 100 \text{ km}$ ) zone of compression.

#### Estimate of the Viscosities

The nondimensional formulation of our model enables us to solve for the velocity and strain rate fields without the need to evaluate the viscosities of the asthenosphere and the lithosphere, which are poorly constrained. By using the dimensionless parameters and physical constraints on the state of stress at the base of the lithosphere, we can estimate these viscosities. An estimated upper bound for the basal drag is of the order of a few hundred bars [Hager and O'Connell, 1979, 1981]. If we multiply the nondimensional shear traction (equation (32)) by the characteristic parameters, we can set the upper limit of the asthenosphere viscosity to

the order of  $\sim 10^{20} \text{ Pa s}$ . Since our simple models assume homogeneous Newtonian viscosity, and do not consider lateral and vertical changes in the viscosity, we would expect that our estimate may be higher than the viscosity of the upper asthenosphere, but lower than that of the uppermost asthenosphere. Indeed, our viscosity estimate is lower by an order of magnitude than estimates of asthenosphere viscosity ( $10^{21} \text{ Pa s}$ ) derived from postglacial rebound [Cathles, 1975; Peltier and Andreus, 1976], but higher by a factor of 2 than estimates of the viscosity of the uppermost asthenosphere ( $4 \times 10^{19} \text{ Pa s}$ ) [Walcott, 1973; Cathles, 1975]. Because the simple models assume homogeneous Newtonian viscosity, lateral and vertical changes in the viscosity are averaged into an effective viscosity that is used in the models. We use our estimate of the asthenosphere viscosity ( $10^{20} \text{ Pa s}$ ) to estimate the lithospheric viscosity by using the ratio  $\frac{\gamma}{4L}$ . If we take  $L = \frac{1}{10}$ , the viscosity ratio between asthenospheric and lithospheric viscosities is  $\gamma = 1/25$  for the Aegean and  $\gamma = 1/140$  for the Andes. Thus, the lithospheric viscosity is  $\sim 2 \times 10^{21} \text{ Pa s}$  in the Aegean and  $\sim 10^{22} \text{ Pa s}$  in the Andes.

A different approach to estimating the effective viscosities is from consideration of buoyancy forces that affect the lithosphere. In the Andes, the observed topography allows the magnitude of the buoyancy forces to be estimated (equation (8)). If the buoyancy forces affect the Andean deformation, where strain rates are of the order of  $10^{-16} \text{ s}^{-1}$ , and the variations of crustal thickness are of the order of 10–30 km, we estimate the effective viscosity as  $1\text{--}3 \times 10^{22} \text{ Pa s}$ . Similarly, if the Aegean is strained at a few times  $10^{-15} \text{ s}^{-1}$  in response to buoyancy forces of a few times  $10^{12} \text{ N m}^{-1}$  [Le Pichon, 1983; England, 1986], then the effective viscosity of the Aegean lithosphere must be about  $10^{22} \text{ Pa s}$ .

Our estimate of the effective viscosities is obtained from two independent methods which give similar results. Comparing the two lithospheric viscosities shows that the Aegean lithosphere is less viscous than the Andean lithosphere. This result agrees with calculations of the strength of continental lithosphere [Sonder and England, 1986], which indicate a weaker and less viscous lithosphere in the Aegean than for lithosphere subjected to compression such as in Tibet or the Andes.

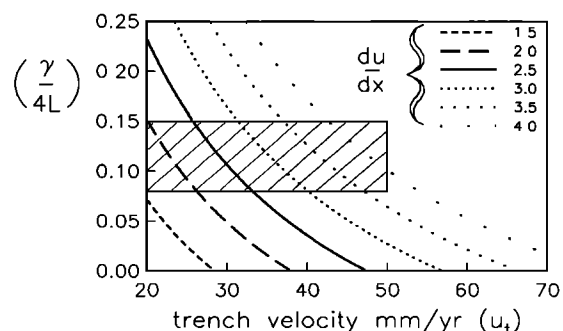


Fig. 11. Contours of extensional strain rate ( $\times 10^{-15} \text{ s}^{-1}$ ) at a distance of 500 km from the wedge tip for different values of  $\frac{\gamma}{4L}$  and  $u_t$  ( $D = 600 \text{ km}$  and  $\theta_0 = 35^\circ$ ). The range ( $1.5 \times 10^{-15} \text{ s}^{-1}$  to  $4.0 \times 10^{-15} \text{ s}^{-1}$ ) corresponds to the range of strain rate in the northern Aegean estimated from seismic studies (see text). The hatched region indicates the range of  $\frac{\gamma}{4L}$  and  $u_t$  for which a narrow zone ( $\leq 100 \text{ km}$ ) of compression is found near the wedge tip (see Figure 12).

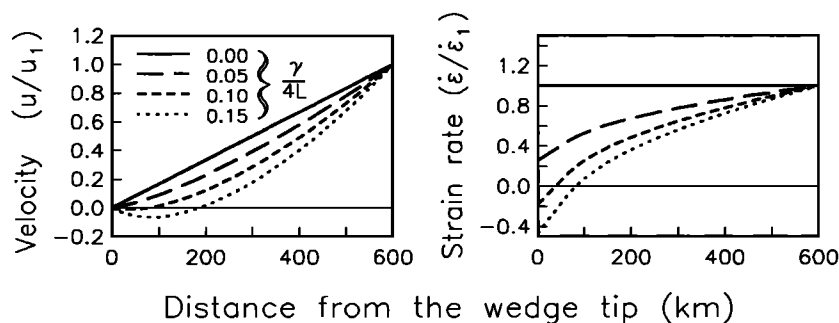


Fig. 12. Solutions for the boundary conditions for the Aegean with various values of  $\frac{\gamma}{4L}$  ( $D = 600$  km,  $\theta_0 = 35^\circ$  and  $u_t = 35$  mm yr $^{-1}$ ). The velocities are scaled by the velocity at the far field ( $u_1 = |u(1)|$ ), and the strain rates are scaled by the strain rate at the far field ( $\dot{\epsilon}_1 = |\dot{\epsilon}(1)|$ ). A narrow zone ( $\leq 100$  km) of compression occurs when  $\frac{\gamma}{4L}$  is in the range 0.08–0.15.

### Limitations of the Model

The continuum models presented above are highly simplified. They investigate only the influence of basal drag resulting from asthenosphere flow within a subduction zone on the overlying continental lithosphere that is subjected to horizontal forces applied at the plate boundary. This simple model yields analytical solutions which give insight into the physical processes of lithospheric deformation above subduction zones, but it neglects other processes that may be important. First, we assumed that the lithosphere and the asthenosphere behave as linear viscous fluids over long periods of time. Experimental and theoretical studies of rock deformation [e.g., *Ashby and Verrall, 1977*] indicate that silicates under the temperature and pressure conditions of the lithosphere and upper mantle may deform by power law creep. Indeed, models that consider nonlinear rheology for the lithosphere [e.g., *England and McKenzie, 1982; Houseman and England, 1986*] and for the asthenosphere [e.g., *Tovish et al., 1978*] may describe the deformation better than linear rheology models. Nevertheless, our use of a linear model, which allows the separation of various effects (Figure 3), has identified the important effects and provides a basis for investigations of more complex models.

Second, the long shape of subduction zones was used to assume two-dimensional flow in the model. When the model is applied to the Andes, the two-dimensional assumption holds nicely. However, the small radius and the relatively high curvature of the Hellenic arc suggest that the two-dimensional assumption is less valid for the Aegean. Thus, future models should include a three-dimensional distribution of the flow. Finally, we considered a homogeneous lithosphere and ignored any body forces due to density differences, such as between the crust and the mantle. Similarly, we did not consider buoyancy forces in the asthenospheric wedge, which may influence the corner flow used in the calculations. Gravitational forces due to thinning or thickening of the crust are neglected and should be included in future models.

Continuum models of large-scale continental deformation that use the standard thin viscous sheet formulation [e.g., *England et al., 1985; Houseman and England, 1986*] suggest that the length scale is determined by the rheology of the lithosphere in conjunction with the length of the plate or that it is determined by the interaction of continuing de-

formation with lithospheric buoyancy forces. In our two-dimensional models there is no characteristic plate width to determine the length scale. In addition we omitted the nonlinear rheology and the buoyancy forces which can determine a horizontal length. Therefore in this study, horizontal length scale is not determined by the deformation, but is specified a priori.

### CONCLUSIONS

The continuum models presented above combine the thin viscous sheet and the corner flow models. The continental lithosphere is described by a two-dimensional thin sheet model that considers basal drag resulting from the viscous asthenosphere flow underneath. A corner flow model with a deforming overlying plate and a rigid subducting plate is used to calculate the shear traction that acts on the base of the lithosphere above a subduction zone. The two models are solved simultaneously for the velocity and strain rate fields within the overlying continental lithosphere by using a perturbation method. The simple form of the model allows analytical solutions which give us insight into the physical processes within a subduction zone.

We apply the models to the Andes and the Aegean, which represent compressional and extensional tectonic environments above subduction zones. For the Andes, the model predicts that a wide region of uplifted topography develops above a steeply dipping slab and a narrower mountain belt develops above a shallowly dipping slab, as observed from the various segments of the central Andes. For the Aegean, the model predicts extension in most of the area and a narrow zone of compression near the trench, as observed. Comparison between the model and the state of stress in the lithosphere enables us to estimate the effective viscosities of the lithosphere and the asthenosphere. The range of asthenospheric viscosity required to produce the observed features is a few times  $10^{20}$  Pa s. The lithospheric viscosity is estimated as a few times  $10^{21}$  Pa s in the Aegean and a few times  $10^{22}$  Pa s in the Andes.

For both regions, the calculated strain rates are in agreement with the observed strain rate derived from seismicity and geological considerations. Our model explains some of the features of the deformation in the Andes and the Aegean that have heretofore not been explained by other models. In particular, our results predict a relation between the width

of the Andes and the dip of the subducting slab in South America. At present, there are no observations to compare with the velocity field calculated by our models. However, the calculated velocities may be tested in the near future with highly accurate geodetic measurements.

#### APPENDIX: THE ACCURACY OF THE THIN SHEET APPROXIMATION WITH BASAL DRAG

One of the assumptions used in the standard thin viscous sheet model is that the top and base of the lithosphere are traction free [England and McKenzie, 1982; Houseman and England, 1986]. When shear traction is added to the base of the lithosphere, the assumption of zero vertical shear strain rates ( $\dot{\epsilon}_{xz} = \dot{\epsilon}_{yz} = 0$ ) and zero vertical shear stress ( $\tau_{xz} = \tau_{yz} = 0$ ) is less accurate. If we continue to follow the thin sheet approximation (as we do in the text) we neglect the shear stresses in the horizontal component of (1) and in the rest of our calculations. The purpose of this appendix is to evaluate the accuracy of the thin sheet approximation by comparing the thin viscous sheet solutions with appropriate two-dimensional calculations.

We assume that the shear traction ( $T_{xz}$ ) that acts on the base of the lithosphere propagates into the lithosphere. Hence, the shear stress ( $\tau_{xz}$ ) has the following form:

$$\tau_{xz}(x, z) = -T_{xz}(x)f(z) \quad (\text{A1})$$

where  $f(z)$  is an arbitrary function and the negative sign comes from the direction of the normal at the base of the lithosphere which, in our coordinate system, is pointing upwards. We choose to represent  $f(z)$  as a power series:

$$f(z) = a_0 + a_1z + a_2z^2 + a_3z^3 + \dots \quad (\text{A2})$$

Since  $0 < z < L$  and  $L \ll 1$  ( $L$  is the ratio between the thickness and the length scale of the lithosphere,  $L \approx 0.1-0.01$ ), we can linearize (A2). We use two boundary conditions, free surface at the top of the lithosphere ( $z = L$ ) and the value of the shear traction at the base ( $z = 0$ ), to get

$$\tau_{xz}(x, z) = -T_{xz}(x) \left[ 1 - \frac{z}{L} + O(z^2) \right] \quad (\text{A3})$$

We follow the same calculations as in the model section, but without the use of the thin sheet approximation. The exact expression for the pressure is

$$p = \tau_{zz} + \int_z^L \tau_{xz,x} dz - \int_z^L \rho g dz \quad (\text{A4})$$

Substituting (A3) and (A4) into the horizontal component of the force balance equation (1), we get

$$2\tau_{xx,x} + \tau_{xz,z} = -T_{xz}(x)_{,xx} \left[ \frac{L}{2} - z + \frac{z^2}{2L} + O(z^3) \right] \quad (\text{A5})$$

As in the thin sheet calculations, we integrate over the thickness to get

$$\frac{d}{dx} [2L\bar{\tau}_{xx}] = T_{xz}(x) - T_{xz}(x)_{,xx} \left[ \frac{L^2}{6} + O(L^4) \right] \quad (\text{A6})$$

where  $\bar{\tau}_{xx}$  is the average stress over the thickness of the lithosphere. In the case of linear rheology we can use the constitutive relations to get

$$\frac{d}{dx} \left[ 4L\eta \frac{d\bar{u}}{dx} \right] = T_{xz}(x) - T_{xz}(x)_{,xx} \left[ \frac{L^2}{6} + O(L^4) \right] \quad (\text{A7})$$

where  $\bar{u}$  is the horizontal velocity averaged over the thickness. The integral form of the velocity is

$$\bar{u} = \frac{1}{4L\eta} \int \int T_{xz}(x) d^2x - \frac{1}{4L\eta} T_{xz}(x) \left[ \frac{L^2}{6} + O(L^4) \right] \quad (\text{A8})$$

We calculated a full two-dimensional flow with two independent methods (stream function and propagator matrix) to evaluate an exact expression for the averaged horizontal velocity. For a flow that is deforming by periodic shear traction at the base of the lithosphere, the exact solution is

$$\bar{u} = \frac{1}{4L\eta} \left( -\frac{1}{k^2} \right) \left[ \frac{2kL \cosh kL}{kL + \sinh kL \cosh kL} \sin kx \right] \quad (\text{A9})$$

where  $k$  is the wave number of the shear traction disturbance. The difference between the approximate solution of the thin viscous sheet model and the exact solution is

$$\lambda(L) = \frac{2kL \cosh kL}{kL + \sinh kL \cosh kL} \quad (\text{A10})$$

For  $L \rightarrow 0$  the factor  $\lambda$  goes to 1. In case of lithosphere with  $L = \frac{1}{10}$  that is deformed by a shear traction with a longwave length ( $k = 2\pi$ ), the value of the factor is  $\lambda(\frac{1}{10}) = 1.0539$ . That means that the thin sheet approximation is off by about 5%. If we rewrite (A9) as a power series, we get

$$\bar{u} = \frac{1}{4L\eta} \left( -\frac{1}{k^2} \right) \left[ 1 + \frac{k^2 L^2}{6} - \frac{29}{360} k^2 L^2 + O(L^6) \right] \sin kx \quad (\text{A11})$$

The first two terms of the power series are identical to the linearized solution of (A8) when  $T_{xz}(x) = \sin kx$ .

*Acknowledgments.* We are grateful to Richard I. Walcott, Gregory Houseman, the JGR associate editor, and Joann Stock for helpful comments and to Göran Ekström for some of the graphics. This work was supported by NASA grant NAG5-840.

#### REFERENCES

- Asby, M. F., and R. A. Verrall, Micromechanisms of flow and fracture, and their relevance to the rheology of the upper mantle, *Philos. Trans. R. Soc. London, ser. A*, 288, 59-95, 1977.
- Barazangi, M., and B. L. Isacks, Spatial distribution of earthquakes and subduction of the Nazca plate beneath South America, *Geology*, 4, 686-692, 1976.
- Batchelor, G. K., *An Introduction to Fluid Dynamics*, Cambridge University Press, New York, 1967.
- Bird, P., Laramide crustal thickening event in the Rocky Mountain foreland and Great Plains, *Tectonics*, 3, 741-758, 1984.
- Bird, P., Formation of the Rocky Mountains, western United States: A continuum computer model, *Science*, 239, 1501-1507, 1988.
- Bird, P., and J. Baumgardner, Fault friction, regional stress, and crust-mantle coupling in southern California from finite element models, *J. Geophys. Res.*, 89, 1932-1944, 1984.
- Burchfield, B. C., and G. A. Davis, Nature and controls of Cordilleran orogenesis, western United States: Extensions of an earlier synthesis, *Am. J. Sci.*, 275-A, 363-396, 1975.
- Cathles, L. M., III, *The viscosity of the Earth's mantle*, Princeton University Press, Princeton, N. J., 1975.
- Chase, C. G., Plate kinematics: The Americas, east Africa, and

- the rest of the world, *Earth Planet. Sci. Lett.*, *37*, 355–368, 1978.
- Dalmayrac, B., and P. Molnar, Parallel thrust and normal faulting in Peru and constraints on the state of stress, *Earth Planet. Sci. Lett.*, *55*, 473–481, 1981.
- Dewey, J. F., and J. M. Bird, Mountain belts and the new global tectonics, *J. Geophys. Res.*, *75*, 2625–2647, 1970.
- Dziewonski, A. M., and J. H. Woodhouse, An experiment in systematic study of global seismicity: Centroid-moment-tensor solutions for 201 moderate and large earthquakes of 1981, *J. Geophys. Res.*, *88*, 3247–3271, 1983.
- Dziewonski, A. M., T. Chou, and J. H. Woodhouse, Determination of earthquake source parameters from waveform data for studies of global and regional seismicity, *J. Geophys. Res.*, *86*, 2825–2852, 1981.
- Ekström, G., and P. C. England, Seismic strain rates in regions of distributed continental deformation, *J. Geophys. Res.*, in press, 1989.
- England, P. C., Comment on “Brittle failure in the upper mantle during extension of continental lithosphere” by Dale S. Sawyer, *J. Geophys. Res.*, *91*, 10487–10490, 1986.
- England, P. C., and G. A. Houseman, Finite strain calculations of continental deformation, 2, comparison with the India-Asia collision zone, *J. Geophys. Res.*, *91*, 3664–3676, 1986.
- England, P. C., and D. P. McKenzie, A thin viscous sheet model for continental deformation, *Geophys. J. R. Astron. Soc.*, *70*, 295–321, 1982.
- England, P. C., G. A. Houseman, and L. J. Sonder, Length scales for continental deformation in convergent, divergent, and strike-slip environments: Analytical and approximate solutions for a thin viscous sheet model, *J. Geophys. Res.*, *90*, 3551–3557, 1985.
- Fenner, R. T., On local solutions to non-Newtonian slow viscous flows, *Int. J. Non-Linear Mech.*, *10*, 207–214, 1975.
- Forsyth D., and S. Uyeda, On the relative importance of driving forces of plate motion, *Geophys. J. R. Astron. Soc.*, *43*, 163–200, 1975.
- Froidevaux, C., and B. L. Isacks, The mechanical state of the lithosphere in the Altiplano-Puna segment of the Andes, *Earth Planet. Sci. Lett.*, *71*, 305–314, 1984.
- Hager, B. H., and R. J. O’Connell, Kinematic models of large-scale mantle flow, *J. Geophys. Res.*, *84*, 1031–1048, 1979.
- Hager, B. H., and R. J. O’Connell, A simple global model of plate dynamics and mantle convection, *J. Geophys. Res.*, *86*, 4843–4867, 1981.
- Hager, B. H., R. J. O’Connell, and A. Raefsky, Subduction, back-arc spreading and global mantle flow, *Tectonophysics*, *99*, 165–189, 1983.
- Hamilton, W., Mesozoic California and underflow of Pacific mantle, *Geol. Soc. Am. Bull.*, *80*, 2409–2430, 1969.
- Houseman, G. A., and P. C. England, Finite strain calculations of continental deformation, 1, Method and general results for convergent zones, *J. Geophys. Res.*, *91*, 3651–3663, 1986.
- Hyndman, R. D., Plate motion relative to the deep mantle and the development of subduction zones, *Nature*, *238*, 263–265, 1972.
- Isacks, B. L., Uplift of the central Andean Plateau and bending of the Bolivian Orocline, *J. Geophys. Res.*, *93*, 3211–3231, 1988.
- Jackson, J. A., and D. P. McKenzie, The relationship between plate motions and seismic moment tensors, and the rates of active deformation in the Mediterranean and Middle East, *Geophys. J. R. Astron. Soc.*, *93*, 45–73, 1988.
- James, D. E., Andean crustal and upper mantle structure, *J. Geophys. Res.*, *76*, 3246–3271, 1971.
- Karig, D. E., Origin and development of marginal basins in the western Pacific, *J. Geophys. Res.*, *76*, 2542–2561, 1971.
- Le Pichon, X., Land-lock oceanic basins and continental collision, in *Mountain Building Processes*, edited by K. Hsü, 201–211, Academic, San Diego, Calif., 1983.
- Le Pichon, X., and J. Angelier, The Hellenic arc and trench system: A key to neotectonic evolution of the eastern Mediterranean area, *Tectonophysics*, *60*, 1–42, 1979.
- Le Pichon, X., and J. Angelier, The Aegean Sea, *Philos. Trans. R. Soc. London, Ser. A*, *300*, 357–372, 1981.
- McKenzie, D. P., Speculations on the consequences and causes of plate motions, *Geophys. J. R. Astron. Soc.*, *18*, 1–32, 1969.
- McKenzie, D. P., Active tectonics of the Alpine-Himalayan Belt: The Aegean Sea and surrounding regions, *Geophys. J. R. Astron. Soc.*, *55*, 217–254, 1978.
- Minster, J. B., and T. H. Jordan, Present-day plate motion, *J. Geophys. Res.*, *83*, 5331–5354, 1978.
- Moffat, H. K., Viscous and resistive eddies near a sharp corner, *J. Fluid Mech.*, *18*, 1–18, 1964.
- Molnar P., and T. Atwater, Interarc spreading and Cordilleran tectonics as alternates related to the age of subducted oceanic lithosphere, *Earth Planet. Sci. Lett.*, *41*, 330–340, 1978.
- Papazachos, B. C., Distribution of seismic foci in the Mediterranean and surrounding area and its tectonic implication, *Geophys. J. R. Astron. Soc.*, *33*, 421–430, 1973.
- Peltier W. R., and J. T. Andrews, Glacial-isostatic adjustment, I, The forward problem, *Geophys. J. R. Astron. Soc.*, *46*, 605–646, 1976.
- Roeder, D., Andean-age structure of eastern Cordillera (province of La Paz, Bolivia), *Tectonics*, *7*, 23–39, 1988.
- Sleep, N., and N. Toksöz, Evolution of marginal basins, *Nature*, *233*, 548–550, 1971.
- Smalley, R. F., Jr., and B. L. Isacks, A high-resolution local network study of the Nazca Plate Wadati-Benioff Zone under western Argentina, *J. Geophys. Res.*, *92*, 13,903–13,912, 1987.
- Sonder, L. J., and P. C. England, Vertical averages of rheology of the continental lithosphere: Relation to thin sheet parameters, *Earth Planet. Sci. Lett.*, *77*, 81–90, 1986.
- Sonder, L. J., and P. C. England, Effects of temperature-dependent rheology on large scale continental extension, *J. Geophys. Res.*, in press, 1989.
- Sonder, L. J., P. C. England, and G. A. Houseman, Continuum calculations of continental deformation in transcurrent environments, *J. Geophys. Res.*, *91*, 4797–4810, 1986.
- Stauder, W., Subduction of the Nazca Plate under Peru as evidenced by focal mechanisms and by seismicity, *J. Geophys. Res.*, *80*, 1053–1064, 1975.
- Stevenson, D. J., and J. S. Turner, Angle of subduction, *Nature*, *270*, 334–336, 1977.
- Suárez, G., P. Molnar, and B. C. Burchfiel, Seismicity, fault plane solutions, depth of faulting, and active tectonics of the Andes of Peru, Ecuador, and southern Colombia, *J. Geophys. Res.*, *88*, 10,403–10,428, 1983.
- Tovish, A., G. Schubert, and B. P. Luyendyk, Mantle flow pressure and the angle of subduction: Non-Newtonian corner flows, *J. Geophys. Res.*, *83*, 5892–5898, 1978.
- Uyeda, S., and H. Kanamori, Back arc opening and the mode of subduction, *J. Geophys. Res.*, *84*, 1049–1061, 1979.
- Walcott, R. I., Flexural rigidity, thickness, and viscosity of the lithosphere, *J. Geophys. Res.*, *75*, 3941–3954, 1970.
- Walcott, R. I., Structure of the Earth from glacio-isostatic rebound, *Annu. Rev. Earth Planet. Sci.*, *1*, 15–37, 1973.
- Wilson, J. T., and K. Burke, Two types of mountain building, *Nature*, *239*, 448–449, 1972.

P. England, Department of Earth Sciences, Park Road, Oxford, OX1 3PR, England.

R. J. O’Connell and S. Wdowinski, Department of Earth and Planetary Sciences, 20 Oxford street, Cambridge MA 02138.

(Received December 28, 1988;  
revised May 4, 1989;  
accepted May 4, 1989.)